

# String Abstractions for Qubit Mapping

Blake Gerard  
The University of Oklahoma  
blake.gerard@ou.edu

Martin Kong  
The University of Oklahoma  
mkong@ou.edu

## Abstract

One of the key compilation steps in Quantum Computing (QC) is to determine an initial logical to physical mapping of the qubits used in a quantum circuit. The impact of the starting qubit layout can vastly affect later scheduling and placement decisions of QASM operations, yielding higher values on critical performance metrics (gate count and circuit depth) as a result of quantum compilers introducing SWAP operations to meet the underlying physical neighboring and connectivity constraints of the quantum device.

In this paper we introduce a novel qubit mapping approach, string-based qubit mapping. The key insight is to prioritize the mapping of logical qubits that appear in longest repeating non-overlapping substrings of qubit pairs accessed. This mapping method is complemented by allocating qubits according to their global frequency usage. We evaluate and compare our new mapping scheme against two quantum compilers (QISKIT and TKET) and two device topologies, the IBM Manhattan (65 qubits) and the IBM Kolkata (27 qubits). Our results demonstrate that combining both mapping mechanisms often achieve better results than either one individually, allowing us to best QISKIT and TKET baselines, yielding between 13% and 17% average improvement in several group sizes, up to 32% circuit depth reduction and 63% gate volume improvement.

**Keywords:** quantum computing, qubit placement, circuit depth optimization, sub-string detection

## 1 Introduction

The field of Quantum Computing (QC) is rapidly growing. Several technologies and applications are being sought and designed to demonstrate Quantum Supremacy [2]. At the same time, various quantum computers have been constructed and made accessible to the public as cloud services [10]. Numerous real quantum devices such as Google Sycamore and

Rigetti's Aspen-9 [18] have been proposed to tackle problems beyond the computational power of today's supercomputers. This effort has been complemented by multiple applications being expressed using frameworks such as OpenFermion [14], while various quantum compilers (QISKIT [9], Rigetti's Pyquil [17], Google's Cirq [7], Cambridge's TKET [21]) support the task of translating and mapping quantum programs onto real hardware.

Ultimately, programs are lowered to a form of quantum assembly such as OpenQASM [6] and used as input to the rest of the quantum compilation process (or "transpilation" in QISKIT terminology). Compiling quantum programs involves several steps, including determining the initial qubit layout, introducing special operations to move the state of a qubit (Quantum Bit) between non-physically adjacent qubits (also known as layout synthesis or routing), gate scheduling, and further lowering the program to technology dependent, native operations available in the physical device, e.g. pulse compilation [1] [22].

In this paper we focus on the problem of determining the initial qubit layout, that is, the task of assigning each logical qubit to a physical qubit on an specific target device. In particular, a quantum computer has a fixed number of physical qubits,  $Q$ , which are physically connected by the underlying technology. Thus, the quantum device is often represented as a coupling graph  $G = (Q, E)$ . The existence of an edge in the graph denotes that the qubits connected by it can be used as operands to a two-qubit quantum gate operation. In this scenario we say that the qubits are "physically adjacent". However, when this is not the case, and owing to the "no cloning theorem" [4], the compiler is required to introduce special quantum operations, SWAPs, to exchange the state between two non-physically adjacent qubits.

Given the number of physical qubits of a device,  $Q$ , the number of possible layouts is  $Q!$ . Given this, the problem of determining a logical-to-physical qubit mapping consists on computing a permutation of the original logical qubit sequence  $q_0, q_1, \dots, q_{n-1}$  so that quality and performance metrics (e.g. circuit depth, gate volume, total error and even execution time) are optimized.

We propose a new qubit mapping class, String-Based Qubit Allocation (SBQA). The key insight is to prioritize qubit allocation over sub-string sequences, and within these, further favor qubits that are heavily used. Strings are extracted from a linearized sub-trace of the quantum program consisting of only indices used in two-qubit gates. Once the *high-impact qubits* are processed within a sub-string, repeated

---

Permission to make digital or hard copies of part or all of this work for personal or classroom use is granted without fee provided that copies are not made or distributed for profit or commercial advantage and that copies bear this notice and the full citation on the first page. Copyrights for third-party components of this work must be honored. For all other uses, contact the owner/author(s).

© 2021 Copyright held by the owner/author(s).  
ACM ISBN 978-x-xxxx-xxxx-x/YY/MM.  
<https://doi.org/10.1145/nnnnnnn.nnnnnnn>

occurrences are removed from the sub-trace before locating the next repeated sub-string to target. This approach is then complemented with a simple qubit allocation using global histograms. Our results show that our qubit mapping strategies often achieve 13%-15% average improvement on several groups of quantum circuits (arranged by size), peaking at 32% circuit depth improvement and 63% in gate volume.

To summarize, the contributions of our work are: i) We propose two new qubit mapping techniques, Sub-String (SS) and Global Frequencies (GF), which are designed to be used both in combination or in stand-alone fashion. In particular, SS is, to the best of our knowledge, the first qubit mapping technique driven by string patterns. ii) We conduct a comprehensive evaluation of our techniques, comparing to layout methods available in state-of-the-art quantum compilers (QISKIT and TKET). Furthermore, we demonstrate that a two-phase qubit mapping strategy offers benefits above any of the individual techniques we propose. iii) To address the urgency for more scalable techniques, we strongly motivate the need for novel qubit mapping strategies by identifying limitations of current qubit/gate mappers. We thus depart from graph- and solver-based approaches. Moreover, we demonstrate that techniques available today are better tuned for small circuits and small quantum devices. iv) We introduce a new standalone tool that can be used by the community to explore new qubit mapping strategies.

The rest of this paper is organized as follows. Section 2 further motivates our research problem. Section 3 covers the main background and related concepts needed. Section 4 provides an overview and working example applying our technique. Section 5 introduces our string-based qubit mapping methods. Section 6 presents a comprehensive evaluation and comparison of our method against baseline compilers, initial layout and routing methods. Section 7 recaps and summarizes the most recent and relevant related work to the problem of qubit mapping. Finally, Section 8 presents the conclusions and future directions of our work.

## 2 Motivation

Numerous techniques proposed in prior work have simultaneously addressed the qubit mapping and routing problem. However, we make the distinction between finding a good initial logical-to-physical qubit mapping (which can change during the compilation of the program) and the process of introducing SWAP operations to amend physical connectivity constraints not met naturally in the program. We thus defer the *routing problem* to already available passes in today's quantum compilers.

To the best of our knowledge, all quantum compilation passes operate over the dependence graph extracted from the quantum assembly representation. TKET's Graph Placement [5] attempts to map logical qubits in a greedy fashion by building graphs from independent pairs of qubits accessed

through various *time steps* (a logical partition of gates that can be executed in parallel). Once the graph is built, it finds an isomorphic sub-graph in the coupling graph representing the physical device. In particular, this method ensures that *only* two timesteps are free of SWAP operations. The algorithm also breaks *long lines* that fail to map into smaller ones until they are successfully assigned. In a similar spirit, MUQUT [3] attempts to map qubits by extracting sub-graphs of fixed cardinality from the program's dependence graph and proceeding to map them to isomorphic sub-graph of the coupling graph. Seed nodes used for extracting the logical sub-graph are randomly selected. Maslov, Falconer and Mosca [13] proposed one of the earliest qubit placement heuristics based on recursive graph partitioning. Techniques like Dense Layout [9] in QISKIT map qubits by searching for the "most connected subset of (logical) qubits". Zulehner, Paler and Wille [25] partition the input program dependence graph into network layers, and apply A\* search techniques to find local optimal mappings; Mappings between adjacent layers are then repaired in a later pass. Siraichi et al. [20] select the initial mapping by determining heavily used logical qubits, and mapping them to physical ones that most closely match their out-degree. A second class of approaches, which incur an even higher computational complexity, resort to Integer Linear Programming and Satisfiability Modulo Theory (SMT) solvers to find optimal solutions; The qubit (and gates) mapping problem is formulated to assign individual gates onto the graph defining the connectivity of a quantum device [15, 16, 22, 24], making it even harder to decouple a strong initial mapping from gate scheduling and mapping.

**A simple example.** To further motivate the need for better qubit mapping techniques, consider the rd84\_253 quantum circuit from the IBM-QX circuit set [11]. This circuit consists of 13,659 quantum gates, of which 5,960 are two-qubit gates. Previous studies have shown that two-qubit gates, significantly impact several quality metrics of quantum programs [22, 23] owing to the topological constraints that must be met for a two-qubit gate to be executed. More precisely, a two-qubit gate can only be executed on two qubits that are physically linked in the coupling graph that defines the quantum device.

We have designed two complementary qubit mapping techniques, one based on *Sub-String* (SS) detection of two-qubit quantum operations, and a *Global Frequency* (GF) approach. Furthermore, when applied back-to-back, the combined mapping strategy, *Global Sub-string Frequency* (GSF), often delivers stronger results than any one individual technique. To demonstrate this, we present in Table 1 excerpts of our results: the variation in circuit depth (number of quantum operations in the critical path), variation in gate volume (number of gates) and variation in SWAP operations (state exchange between two any qubits). Results are normalized to the baseline compiler QISKIT using the SABRE initial layout

method and TKET with *Noise-Aware Placement*. For circuit depth and gate volume, any value above 1.00 represents an improvement, while for the SWAP Ops, positive values indicate improvement. Each of our three mapping methods are compiled with a *base* configuration (suffix *b*) and with an *optimized* one (suffix *o*) – Flags used shown in Section 6. As we can see, our methods achieve up to 1.19× circuit depth improvement with QISKIT and up to 1.20× with TKET. At the same time, with GSF<sub>o</sub> on TKET, we produce up to 1.25× improvement on the gate volume metric, out matching all other mappings. Lastly, our mapping methods also improves the number of needed SWAP operations, obtaining a 29% reduction with GSF<sub>o</sub>. As a point of reference the best improvement in gate volume reported in [12] was 30% on a circuit with 3,888 QOPS (quantum operations) while for rd84\_253 the improvement on gate volume was 5%. Lastly, the same study was limited to circuits with up to 34,881 gates.

**Table 1.** rd84\_253 compilation metrics collected on IBM Manhattan (65 qubit): Circuit Depth, Gate Volume and Inserted SWAP Operations.

Metric	Compiler Config.	Mapping Method					
		SS <sub>b</sub>	SS <sub>o</sub>	GF <sub>b</sub>	GF <sub>o</sub>	GSF <sub>b</sub>	GSF <sub>o</sub>
Circuit Depth	QISKIT	1.19	1.01	1.19	1.03	1.17	1.05
	TKET	1.02	1.07	0.96	1.12	1.09	1.2
Gate Volume	QISKIT	0.67	1.01	0.7	1.04	0.65	1.07
	TKET	0.097	1.1	0.96	1.14	1.03	1.25
SWAPS Ops	QISKIT	-0.47	0.01	-0.4	0.04	-0.51	0.06
	TKET	0.19	0.16	0.17	0.17	0.28	0.29

### 3 Background

**Qubits.** Qubits are the basic unit of information in quantum computing. Each qubit represents a linear combination  $c_1|0\rangle + c_2|1\rangle$  of two basis states  $|0\rangle$  and  $|1\rangle$ , with  $c_1$  and  $c_2$  being complex numbers. A set of logically contiguous qubits conforms a *quantum register*.

**Quantum Gates.** Are unitary matrix operations applied to individual qubits. Current quantum gate typically operate on a single qubit and on two qubits at the time. For example, the CX (Controlled-NOT) gate takes two operands, the *control qubit* and the *target qubit*, while the X gate takes a single qubit. Each quantum architecture defines a *gate basis*, a set of gates to which all programs must be reduced to. For example, IBM quantum computers use gates CX, ID, RZ, SX and X as their gate basis.

**Quantum Assembly and Circuit Diagrams.** Quantum programs can be represented in a device agnostic fashion using quantum assembly formats such as OpenQASM [6]. Listing 1 show the implementation of the graycode6\_47 circuit using OpenQASM. The same program can also be

visualized as a *circuit diagram*, as shown in Figure 1. Circuit diagrams depict logical qubits as horizontal lanes, with the time-dimension advancing from left to right. Single-qubit gates are directly placed on a single lane, while two-qubit gates connect the qubit lanes used as operands.

```

OPENQASM 2.0;
qreg q[16];
creg c[16];
cx q[1],q[0];
cx q[2],q[1];
cx q[3],q[2];
cx q[4],q[3];
cx q[5],q[4];

```

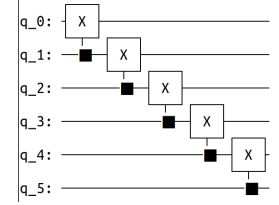


**Figure 1.** Graycode6\_47 circuit diagram.

**Listing 1.** Graycode in OpenQASM.

**Coupling Graph.** Current quantum computers present stringent architectural constraints that require qubits used as arguments to two-qubit gates (e.g. the cx gate) to be qubits that are physically connected. Thus, quantum devices are conceptually modeled in *coupling graphs*. A *physical* qubit in modeled in the graph as a node, while edges linking two nodes establish the physical connection. Figure 2 show the topology of the quantum devices used in our evaluation, the 27-qubit IBM Kolkata and the 65-qubit IBM Manhattan [10].

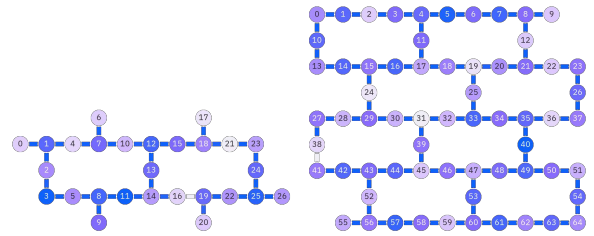


**Figure 2.** Example coupling maps: 27-qubit device IBM Kolkata (left) and 65-qubit IBM Manhattan (right)

### 4 Overview

In this section we give a brief overview of the major steps followed for computing a more effective initial logical-to-physical qubit mapping. The input to our mapping method is a QASM file containing the quantum operations (QOPS), such as the one shown in Fig. 1. Next, we extract a subtrace containing not only the CX (CNOT) gates, but all two-qubit gate operations. Take for instance circuit max46\_240 from the IBM-QX quantum circuit set [11], which consists of 27,126 QOPS, of which 11,844 are CX gates. The remaining gates are distributed as 5,076 TDG gates, 6,768 T gates, 3,384 H gates and 54 X gates. Next, for each 2-qubit gate of the form *OPCODE*  $q_1, q_2$  we compute a linearized identifier  $id_{lin} = q_1 \cdot DEV_{width} + q_2$ , where  $DEV_{width}$  is the number of physical qubits available in target quantum device. Thus,

all symbols conforming our strings will be defined in the alphabet  $\{u \cdot DEV_{width} + v : 0 \leq u, v < DEV_{width}\}$ .

Once the program has been converted into a linearized string representation, we compute a few statistics to drive the qubit mapping process. For example, this program references 76 distinct characters of our alphabet from the potential 729 ( $27^2$ ). These are all the logical qubit-to-qubit connections used the circuit. In total, the 76 logical links are used 11,844 times; The average logical connection is used 155.8 times, with a standard deviation of 174.6. However, not all qubits are used in the same fashion nor at the same frequency. Consider Table 2, where for each logical qubit used in circuit `max46_240` we show in the third row, the number of times that the said qubit is used as the first operand (the control qubit) in a 2-qubit gate. The second row states the number of distinct logical connections used in the program for each logical qubit, while the fourth and last row limit the total number of references to only the two and three most frequently qubits paired with a given qubit  $q_i$ . From here on, we will often refer to all pairs  $\langle q_i, q_j \rangle$  of a given qubit  $q_i$  as the logical pair, edge, link or connections of  $q_i$ .

**Table 2.** Edge histogram of circuit `max46_240`.

Qubit	0	1	2	3	6	7	8	9
No. Distinct	2	6	8	8	9	9	9	9
Used Total	420	1222	1128	972	1010	1636	2060	1876
Top 2	420	1074	732	460	382	752	1304	1188
Top 3	420	1142	912	580	558	972	1644	1360

Next, we proceed to determine if there exists a substring pattern in the linearized string that repeats and which does not overlap with following occurrences. For example, from the linearized string representation of `max46_240` a substring of length 364 meeting these conditions is found 2 times at locations 4,536 and 11,200. This means that there are two sequences of 364 2-qubit gate operations which can be optimized (hopefully) by the quantum compiler only once. The repeated sequence found, from a graph-based mapping approach, could eventually be found as a path (or *line* in TKET terminology) in the data dependence graph, but interspersed with single-qubit gates, making the search for gate sequences of this length much harder to find.

The actual logical to physical mapping of qubits then proceeds. We compute the information listed in Table 2 but restricted to the logical qubits used within the subsequence. Mapping within the gate subsequence will be constrained to only the qubits whose frequency of usage is above the mean value of the subsequence. For example, when limiting this information to only the qubit pairs referenced in the substring, the mean value becomes 849.2; A quick inspection reveals that 5 logical qubits have more logical links than the mean, namely  $q_1, q_2, q_7, q_8$  and  $q_9$ . Qubits that satisfy this

condition belong to the *High-Impact Qubits* (HIQ) set. Furthermore, the steps that follow will limit the mapping of logical qubits that belong to the HIQ set. This is done to avoid mapping qubits that will ultimately have a low impact on later compilation metrics, such as the *gate volume*, *circuit depth* and *swap count*. Mapping takes place by choosing a *leading logical qubit* and a *leading physical qubit* to which to map it. By extension, logical qubits used as the target node to a logical link will be mapped to the qubits physically adjacent to the *lead physical qubit*. Mapping proceeds by sorting and aligning the neighboring qubits in both cases. In our example, logical qubit  $q_8$  and physical qubit  $q_{25}$  would be chosen as the lead qubits, while logical qubits  $q_1, q_7$  and  $q_9$  would be mapped to physical qubits  $q_{22}, q_{24}$  and  $q_{26}$ . We note here that logical qubit  $q_9$  was also in the HIQ set, and was a close second choice of a *lead qubit*. However, selecting  $q_8$  will preclude choosing  $q_9$  later.

Our algorithm will attempt to continue mapping qubits from the HIQ set if the chosen *lead logical qubit* has at least one non-mapped neighbor. If no further mappings take place within the current string subsequence, the current sequence is removed from the linearized string representation prior to repeating the steps starting with the local histogram computation. If no repeating subsequence is found, the string-based qubit allocation strategy terminates, and we proceed to use only the global pair frequencies (See Table 2). Finally, if no qubit pair can be mapped, the process alternates to map most referenced logical qubits to physical qubits with the best fidelity and lowest read error.

## 5 Mapping

### 5.1 Detecting Sub-Strings

As first step, we extract a linearized trace from all the pairs of qubit indices appearing in 2-qubit gates (e.g. (1, 2) from CX 1, 2), and encoding the pair as a  $q_1 \cdot Q_{device} + q_2$ , where  $Q_{device}$  is the number of physical qubits in the quantum device,  $q_1$  is the first component of the pair, and  $q_2$  the second one. The linearization allows us distinguish pairs  $\langle i, j \rangle$  from  $\langle j, i \rangle$ . We do note, however, that all 2-qubit gate operations, regardless of their type, will be encoded in this fashion.

Next, we proceed to determine whether there exists a subsequence of QASM operations that repeats within the linearized two-qubit stream. If a repeating subsequence does exist, we are interested in the longest, non-overlapping one. In summary, we aim to find the *longest repeating non-overlapping substring*. Then, the most relevant qubits within each substring will be mapped first.

Eq. 1 is used to compute the length of matching substrings from a given string  $S$ , and storing the prefix lengths in a table  $T$ . Table  $T$  is built from the bottom-up, computing first prefixes of length 1, then prefixes of length 2 and so on. It is easy to see that if  $S_i \neq S_j$  then the matching prefix length is zero; Otherwise the new prefix length effectively increases

by one. Eq. 1 can be easily implemented in an iterative fashion; However, care must be taken to minimize the memory footprint of  $T$  in order to avoid incurring in a  $O(n^2)$  space complexity, which for QASM-based circuits soon consisting of millions of QOPS can result in significant memory requirements. To illustrate this point, a program with 100K QASM operations, and encoding each qubit index pair as a 4-byte integer would require 32.25GB while one with 500K quantum operations would require 931GB. Thus, when computing this table, we resort to keep only the two most recent rows, keeping the maximum length of  $T_{i,j}$ , and storing the  $i$  index at each update to the maximum length.

$$T_{i,j} = \begin{cases} T_{i-1,j-1} + 1 & : S_i = S_j \wedge j > i \wedge T_{i-1,j-1} < j - i \\ 0 & \text{otherwise} \end{cases} \quad (1)$$

## 5.2 Global Frequencies

Next, We compute for each qubit pair  $\langle q_i, q_j \rangle$  the number of times that such pair is used in two-qubit quantum gates. We denote this value as  $refs(\langle q_i, q_j \rangle)$ . Then, for each qubit  $q_i$  we compute its total usage frequency as:

$$freq(q_i) = \sum_{q_j} refs(\langle q_i, q_j \rangle)$$

In several instances, and to prioritize the mapping of qubits, we will also sort all neighboring qubits  $q_j$ , for a given  $q_i$ , by their  $refs$  value.

## 5.3 Mapping Qubits from Sub-Strings

Algorithm 1 presents the steps taken to map a subset of logical qubits used in the input program to a set of physical available qubits. The overall algorithm proceeds by finding *longest repeating non-overlapping sub-strings* (LRNOS) in the quantum program, and proceeding to map as many *high-impact qubits* (HIQ) as possible from it. We define a HIQ as a qubit with a higher  $freq$  than the mean, but restricted to the current LRNOS. To differentiate HIQ from other qubits, we compute the average number of times that a logical qubit  $q_i$  appears as the first operand of a two-qubit gate operation (e.g.  $CX q_i, q_j$ ), as defined in Sec.5.2. This number is then used as a minimum threshold to properly identify any HIQ. In addition, we also require logical qubits to be in the  $Q_{pending}$  set.

Qubit mapping proceeds at two levels, *rounds* and *steps*. Rounds allocate qubits for a given LRNOS, and are controlled in the outermost while-loop of Alg. 1; Steps perform finer-grain actions in the innermost while-loop, by first selecting a leading physical qubit ( $q_{phys}$ ) to be used as the *control* qubit to a number of 2-qubit gate operations, followed by selecting the still available physical qubits adjacent to the leading one ( $adj(q_{phys})$ ). A similar selection is done for the logical qubits; The lead logical qubit is selected from the  $L_{hiq}$ ,

---

### Algorithm 1 Map Qubits by Sub-String (SS) Method

---

**Input:**  $Q_{phys}$ : Physical Qubit Set;  $Q_{log}$ : Logical Qubit Set;  $P$ : QASM Program

**Output:**  $M_{l2p}$ : Logical-to-physical qubit layout map.

```

1: /* Initialize pending list */
2:  $Q_{pending} \leftarrow$  Extract two-qubit indices from  $P$ ;
3:  $Q_{avail} \leftarrow Q_{phys}$ ;
4:  $edges \leftarrow$  Extract_qubit_pairs_from_program ( $P$ );
5:  $P_{str} \leftarrow$  linearize_qubit_pairs ( $edges$ );
6: while (not done) do
7:   /* Build a histogram of edges (pairs of qubits) */
8:    $H \leftarrow$  build_qubit_edge_frequency ( $edges$ );
9:   /* Select High-Impact Qubits (hiq) from  $H$  */
10:   $L_{hiq} \leftarrow$  build_high_impact_qubit_list ( $H$ );
11:   $str \leftarrow$  find_lrns ( $P_{str}$ );
12:  if length( $str$ ) < 2 then
13:    done  $\leftarrow$  True;
14:  end if
15:   $ehist \leftarrow$  substring_histogram ( $str$ );
16:  while ( $q_{phys} \leftarrow$  get_next_physical_qubit ( $Q_{avail}$ )) do
17:    if ( $q_{phys}$  is invalid) then
18:      break;
19:    end if
20:     $L_{phys} \leftarrow \{q_{phys}\} \cup (adj(q_{phys}) \cap Q_{avail})$ ;
21:     $L_{log} \leftarrow$  select_logical_qubits ( $Q_{pending}, L_{hiq}, ehist$ );
22:
23:    if size( $L_{log}$ ) < 2 then
24:      break;
25:    end if
26:     $M_{l2p} \leftarrow$  map_qubits ( $L_{log}, L_{phys}$ );
27:     $Q_{pending} \leftarrow Q_{pending} - L_{log}$ ;
28:     $Q_{avail} \leftarrow Q_{avail} - L_{phys}$ ;
29:    sort  $Q_{avail}$  by number of available neighbors;
30:  end while
31:  if no qubits were mapped in previous loop then
32:     $P_{str} \leftarrow$  remove_substring_occurrences ( $P_{str}, str$ );
33:    sort  $Q_{avail}$  by number of available neighbors;
34:     $edges \leftarrow edges - \{\langle q_i, q_j \rangle : q_i \text{ or } q_j \notin Q_{pending}\}$ ;
35:  end if
36: end while
37: return  $M_{l2p}$ ;

```

---

after which the  $k = len(adj(q_{phys}))$  most often qubits  $q_j$  such that  $\langle q_i, q_j \rangle$  are chosen and added to  $L_{log}$ . Once logical and physical qubits have been chosen, we map each corresponding leading qubits and their adjacent ones, assigning more heavily used logical qubits to the physical qubits with the lowest error. The *steps* loop exits when either a leading physical qubit cannot be found, or when the set of logical qubits,  $L_{log}$ , consists of only one qubit (the leading one). The latter scenario occurs when non-HIQ qubits remain in the current LRNOS. After exiting the *steps* loop, a few actions

are taken to prepare for the next LRNOS: sub-string occurrences of the current LRNOS are removed from  $P_{str}$ , the set/list of available physical qubits ( $Q_{avail}$ ) is sorted by the number of available neighbors, while the list of linearized qubit pairs ( $edges$ ) is updated by removing all edges that have been partially allocated either because the source or target qubit are not pending anymore.

#### 5.4 Mapping Remaining 2-qubit gate Qubits

---

##### Algorithm 2 Map Qubit by Global Frequency (GF)

---

**Input:**  $Q_{phys}$ : Physical Qubit Set;  $Q_{log}$ : Logical Qubit Set;  $P$ : QASM Program

**Output:**  $M_{l2p}$ : Logical-to-physical qubit layout map.

```

1: /* Initialize pending list */
2:  $Q_{pending} \leftarrow$  Extract two-qubit indices from  $P$ ;
3:  $Q_{pending} \leftarrow Q_{pending} - \text{physical}(M_{l2p})$ 
4: sort  $Q_{avail}$  by number of available physical neighbors;
5:  $edges \leftarrow$  Extract_qubit_pairs_from_program ( $P$ );
6: while ( $Q_{pending} \neq \emptyset$ ) do
7:    $edges \leftarrow edges \cap \{\langle q_i, q_j \rangle : q_i, q_j \in Q_{pending}\}$ ;
8:    $ehist \leftarrow$  build_histogram ( $edges$ );
9:   if  $ehist$  is empty then
10:     break;
11:   end if
12:    $q_{phys} \leftarrow$  get_next_physical_qubit ( $Q_{avail}$ );
13:    $L_{phys} \leftarrow \{q_{phys}\} \cup (adj(q_{phys}) \cap Q_{avail})$ ;
14:    $L_{log} \leftarrow$  select_logical_qubits ( $Q_{pending}, ehist$ );
15:   if  $\text{size}(L_{log}) < 2$  then
16:     break;
17:   end if
18:    $M_{l2p} \leftarrow$  map_qubits ( $L_{log}, L_{phys}$ );
19:    $Q_{pending} \leftarrow Q_{pending} - L_{log}$ ;
20:    $Q_{avail} \leftarrow Q_{avail} - L_{phys}$ ;
21: end while
22: return  $M_{l2p}$ ;

```

---

Next, we present a second algorithm, inspired in MUQUT's [3] k-vertex topology graph extraction, and which complements the sub-string based qubit allocation method introduced in the previous section. Algorithm 2 is a more direct version of Algorithm 1. It only attempts to map qubits by considering the histogram (global frequency) of logical qubits used in 2-qubit gates. Consequently, the assignment of qubits is performed in a single loop, choosing first a leading physical qubit (and indirectly, its adjacent physical ones), followed by selecting the leading logical qubit together with its neighbors. The actual mapping proceeds in the same fashion as in the first algorithm. The loop stops whenever we find that the updated global histogram  $ehist$  has no pending edges (NOTE: qubits can still be pending, but they will no form a pair  $\langle q_i, q_j \rangle$  where both qubits are in the  $Q_{pending}$ ). At the end of each iteration, both the logical pending qubit

set ( $Q_{pending}$ ) and the physical available qubit set ( $Q_{avail}$ ) are accordingly updated.

#### 5.5 Mapping Remaining 1-qubit gate Qubits

If after mapping qubits with Algorithm 1 – 2 no unmapped pair  $\langle q_i, q_j \rangle$  can be found, we then proceed to map qubits based solely on their single-qubit gate error and read error rates, which are obtained from the physical parameter files associated to each quantum device.

## 6 Evaluation

We implemented the qubit mapping methods described in Sec.5 as a single standalone tool which takes quantum circuits in OpenQASM and emits a remapped program also in OpenQASM. The compilers used, together with their version and options are listed in Table 5. Devices used are the IBM Manhattan (65-qubit, 72 edges) and Kolkata (27-qubit, 28 edges) [10]. Physical parameter files were retrieved on August 22, 2021.

**Evaluated Circuits:** We use the IBM-QX QASM benchmark set [11], which has been extensively used in prior works [12, 21, 22, 25]. All circuits in this collection utilize up to 16 qubits. The suite consist of 158 quantum circuits, of which we use all but the *ground-state-estimation* circuit owing to compilers removing all but a handful of operations from a program with 390K quantum operations. The average circuit size (in number of quantum gates) of the remaining 157 circuits is 18,714.5 operations, with a standard deviation of 62,863. However, 105 of the circuits present 1000 or fewer operations. We thus organize our results in 9 groups. The specific ranges of circuit sizes can be found on the leftmost column of Table 3–7. The new mappings were collected in a 32-core AMD Thread-Ripper server, with 128 GB DRAM, and operating with Ubuntu 18. The total time to generate all 157 layouts, for the Manhattan topology, with our SS, GF and GSF mappings was 79.2sec, 79.4sec and 159.3sec, respectively.

### 6.1 General Trends

We focus our analysis on the *circuit depth* (number of gates in the program's critical path) and on the *gate volume* metric (number of gates in the program). However, as in some cases the impact on these metrics can be small relative to the original circuit size, we take the approach of previous works [12, 21, 22] and consider only the metric variation, i.e., the difference between the metric obtained after compilation and the original metric value (circuit depth or gate volume).

We show the summary of our results on Tables 3 – 7. The first column in all four tables indicates the group number (range of circuit sizes prior to compilation) and the number of circuit instances meeting the criterion. The next 12

**Table 3.** Average of normalized depth variation by circuit size – QISKIT compiler.

C1 Group [Size Range] : (Instances):	IBM Manhattan (65 qubit)						IBM Kolkata (27 qubit)					
	C2 SS <sub>b</sub>	C3 SS <sub>o</sub>	C4 GF <sub>b</sub>	C5 GF <sub>o</sub>	C6 GSF <sub>b</sub>	C7 GSF <sub>o</sub>	C8 SS <sub>b</sub>	C9 SS <sub>o</sub>	C10 GF <sub>b</sub>	C11 GF <sub>o</sub>	C12 GSF <sub>b</sub>	C13 GSF <sub>o</sub>
G1 [ 1: 1K] (105)	1.01	1.06	1.07	1.01	0.99	1.02	1.03	1.03	1.07	1.08	0.95	1.08
G2 [ 1K: 5K] (15)	1.11	1.03	1.10	1.02	1.12	1.03	1.11	1.02	1.11	1.00	1.12	1.02
G3 [ 5K: 10K] (6)	1.13	0.98	1.15	0.98	1.14	0.98	1.15	0.99	1.13	0.99	1.14	1.00
G4 [10K: 20K] (7)	1.13	1.00	1.13	1.02	1.12	1.02	1.13	1.01	1.12	1.02	1.12	1.01
G5 [20K: 30K] (5)	1.13	0.95	1.12	0.97	1.13	0.97	1.14	1.00	1.16	1.01	1.17	1.00
G6 [30K: 40K] (5)	1.13	1.00	1.11	0.99	1.13	1.00	1.13	0.99	1.12	1.00	1.13	1.02
G7 [40K: 100K] (5)	1.13	0.98	1.13	0.98	1.14	1.00	1.12	0.97	1.14	1.01	1.11	0.99
G8 [100K: 250K] (7)	1.10	1.00	1.11	0.98	1.10	1.00	1.11	0.99	1.11	1.00	1.12	1.00
G9 [250K: 1M] (2)	1.09	0.98	1.09	0.98	1.09	0.98	1.16	1.05	1.14	1.05	1.16	1.05

**Table 4.** Average of normalized depth variation by circuit size – TKET compiler.

C1 Group [Size Range] (Instances):	IBM Manhattan (65 qubit)						IBM Kolkata (27 qubit)					
	C2 SS <sub>b</sub>	C3 SS <sub>o</sub>	C4 GF <sub>b</sub>	C5 GF <sub>o</sub>	C6 GSF <sub>b</sub>	C7 GSF <sub>o</sub>	C8 SS <sub>b</sub>	C9 SS <sub>o</sub>	C10 GF <sub>b</sub>	C11 GF <sub>o</sub>	C12 GSF <sub>b</sub>	C13 GSF <sub>o</sub>
G1 [ 1: 1K] (105)	0.66	0.78	0.71	0.88	0.64	0.75	0.68	0.80	0.70	0.89	0.63	0.72
G2 [ 1K: 5K] (15)	0.89	0.97	0.89	1.02	0.88	0.96	0.79	0.89	0.81	0.90	0.80	0.89
G3 [ 5K: 10K] (6)	0.85	0.97	0.87	0.98	0.84	1.03	0.89	0.97	0.86	1.03	0.88	1.05
G4 [ 10K: 20K] (7)	0.93	1.03	0.91	1.05	0.97	1.10	0.94	1.04	0.90	1.03	0.96	1.05
G5 [ 20K: 30K] (5)	0.99	1.10	1.01	1.12	0.97	1.06	0.97	1.06	0.97	1.07	0.98	1.08
G6 [ 30K: 40K] (5)	0.93	1.04	0.94	1.09	0.93	1.08	0.92	1.00	0.94	1.05	0.94	1.02
G7 [ 40K: 100K] (5)	0.92	1.02	0.92	1.03	0.92	1.02	0.86	0.96	0.88	0.98	0.85	0.96
G8 [100K: 250K] (7)	0.92	1.05	0.93	1.04	0.93	1.04	0.93	1.04	0.92	1.03	0.94	1.05
G9 [250K: 1M] (2)	0.92	1.01	0.98	1.09	0.92	1.01	0.86	0.97	0.87	0.96	0.86	0.97

**Table 5.** Experimental Testbed

Compilers		
	Base Flags / Passes	Opt Flags / Passes
TKET v0.13.0	identity placement + routing + IBM rebase + validity predicate	Same as base + FullPeepholeOptimize + NoiseAwarePlacement (Only for Original QASM)
QISKIT v0.23.6	layout_method= 'trivial' + opt-level=2	layout_method='sabre' + routing_method='sabre' + scheduling_method=None + translation_method= 'translator' + opt-level=2

columns list the average of our normalized results, i.e. the ratio of the metric obtained with the baseline configuration by the metric value obtained when using our mapping (or a combination of them). Column names denote the combination of our 3 mappings (SS, GF, GSF) in tandem with two different compiler configurations, *b* for *base* and *o* for *optimized*. As previously discussed, GSF is the back-to-back application of our two mapping strategies, Sub-String (SS)

followed by Global Frequencies (GF). Columns C2–C7 correspond to results collected on IBM Manhattan while columns C8–C13 correspond to IBM Kolkata.

**Impact on Circuit Depth.** From Table 3 and Table 4 we observe that our qubit mappings are especially beneficial when used in conjunction with the QISKIT compiler, while benefits when utilizing TKET are more noticeable for groups G3–G9, the larger circuit classes. We recall that average values above 1.00 represent an improvement on the metrics. We can also observe an interesting phenomenon between groups G1 and G2 on Table 3, which is an inversion in trends; On group G1 configurations SS<sub>o</sub>, GF<sub>o</sub> and GSF<sub>o</sub> outperform SS<sub>b</sub>, GF<sub>b</sub> and GSF<sub>b</sub>. Then, starting with group G2, the *base* configurations always outperform the *optimized* ones. This demonstrates that, QISKIT is currently better tuned for smaller circuits. In contrast, the same effect is not detected in Table 4, where the *optimized* configurations always outperform the *base* ones. Nonetheless, while a similar inversion does not manifest with TKET, first signs of improvements appear on group G3, and become more consistent on groups G4 – G9. This suggests that TKET’s qubit placement method is better tuned for circuits with up to 10K gates.

**Table 6.** Average of normalized gates variation by circuit size: QISKIT compiler.

C1 Group [Size Range] (Instances):	IBM Manhattan (65 qubit)						IBM Kolkata (27 qubit)					
	C2 SS <sub>b</sub>	C3 SS <sub>o</sub>	C4 GF <sub>b</sub>	C5 GF <sub>o</sub>	C6 GSF <sub>b</sub>	C7 GSF <sub>o</sub>	C8 SS <sub>b</sub>	C9 SS <sub>o</sub>	C10 GF <sub>b</sub>	C11 GF <sub>o</sub>	C12 GSF <sub>b</sub>	C13 GSF <sub>o</sub>
G1 [ 1: 1K] (105)	0.55	1.04	0.63	0.98	0.53	0.98	0.57	1.01	0.63	1.00	0.49	1.00
G2 [ 1K: 5K] (15)	0.63	1.04	0.63	1.04	0.64	1.05	0.64	1.00	0.64	0.99	0.64	1.00
G3 [ 5K: 10K] (6)	0.63	0.98	0.65	0.97	0.64	0.97	0.65	0.98	0.62	0.99	0.64	1.00
G4 [ 10K: 20K] (7)	0.64	1.00	0.64	1.00	0.63	1.02	0.64	1.01	0.63	1.02	0.64	1.01
G5 [ 20K: 30K] (5)	0.64	0.90	0.62	0.94	0.64	0.93	0.64	0.99	0.66	1.01	0.68	1.01
G6 [ 30K: 40K] (5)	0.64	1.00	0.63	1.01	0.64	1.00	0.63	1.00	0.63	1.00	0.63	1.04
G7 [ 40K: 100K] (5)	0.64	0.98	0.64	0.98	0.66	0.99	0.62	0.92	0.65	1.01	0.62	0.97
G8 [100K: 250K] (7)	0.65	1.01	0.66	1.00	0.65	1.01	0.64	0.98	0.64	0.99	0.66	1.01
G9 [250K: 1M] (2)	0.60	0.92	0.60	0.91	0.60	0.92	0.65	1.02	0.63	0.98	0.65	1.02

**Table 7.** Average of normalized gates variation by circuit size – TKET compiler.

C1 Group [Size Range] (Instances):	IBM Manhattan (65 qubit)						IBM Kolkata (27 qubit)					
	C2 SS <sub>b</sub>	C3 SS <sub>o</sub>	C4 GF <sub>b</sub>	C5 GF <sub>o</sub>	C6 GSF <sub>b</sub>	C7 GSF <sub>o</sub>	C8 SS <sub>b</sub>	C9 SS <sub>o</sub>	C10 GF <sub>b</sub>	C11 GF <sub>o</sub>	C12 GSF <sub>b</sub>	C13 GSF <sub>o</sub>
G0 [ 1: 1K] (105)	0.52	0.64	0.59	0.87	0.48	0.64	0.52	0.69	0.56	0.81	0.44	0.57
G1 [ 1K: 5K] (15)	0.78	0.91	0.79	0.97	0.78	0.91	0.71	0.82	0.71	0.83	0.71	0.82
G2 [ 5K: 10K] (6)	0.78	0.96	0.79	0.96	0.76	1.02	0.80	0.99	0.79	1.03	0.80	1.10
G3 [ 10K: 20K] (7)	0.89	1.04	0.88	1.06	0.91	1.11	0.88	1.04	0.86	1.03	0.91	1.05
G4 [ 20K: 30K] (5)	0.94	1.11	0.96	1.12	0.94	1.08	0.92	1.06	0.91	1.07	0.93	1.07
G5 [ 30K: 40K] (5)	0.88	1.07	0.89	1.10	0.88	1.09	0.88	1.01	0.89	1.05	0.89	1.03
G6 [ 40K: 100K] (5)	0.85	1.01	0.85	1.02	0.87	1.00	0.81	0.93	0.80	0.95	0.78	0.94
G7 [100K: 250K] (7)	0.88	1.06	0.88	1.06	0.88	1.05	0.87	1.04	0.85	1.02	0.88	1.05
G8 [250K: 1M] (2)	0.86	1.02	0.93	1.11	0.86	1.02	0.80	0.95	0.79	0.93	0.80	0.95

Next, we note that our results with QISKIT are somewhat better on the Kolkata topology, where we achieve an average circuit depth improvement of up to  $1.17\times$  on G5 and  $1.16\times$  on G9 with GSF<sub>o</sub>. These are good examples of when SS and GF can work in tandem to obtain better overall results. In comparison, results on Manhattan exhibit less variation among groups, and averaging  $1.13\times$  improvement in several groups. Notable improvements with TKET on Manhattan can be seen on group G4, where GSF<sub>o</sub> ( $1.10\times$ ) clearly outmatches SS<sub>o</sub> ( $1.03\times$ ) and GF<sub>o</sub> ( $1.05\times$ ). Finally, we note a modest decline on the effectiveness of our techniques for groups G7–G9 on Manhattan, and a more pronounced one on Kolkata for the same groups.

**Impact on Gate Volume.** Tables 6–7 summarize our results on the gate count variation using both compilers and topologies. The first observation we make is related to the effect of the compiler configurations used *base* and *optimized*; Our methods were particularly impactful on the circuit depth when using the QISKIT compiler. Sadly, this appears to come with a penalty that manifests on the gate volume, where the *base* configurations are consistently outperformed by the *optimized* ones. The phenomenon can be interpreted as additional gates being introduced out of the critical path, but

often enough to yield a 30%–40% gap between the *base* and *optimized* configurations. This trend is not observed when using the TKET compiler, where improvements on both the circuit depth and gate volume correlate. Overall, we also remark that improvements in the gate volume when using QISKIT only allow to match the baseline, whereas with TKET improvements are of the same order as on the circuit depth. For instance, on Manhattan’s group G4, the aggregate improvement when using GSF<sub>o</sub> (i.e. SS<sub>o</sub> + GF<sub>o</sub>) is of the order of  $1.11\times$ , besting the  $1.04\times$  of SS<sub>o</sub> and  $1.06\times$  of GF<sub>o</sub>. In a similar fashion, TKET on Kolkata’s group G3 achieves an average  $1.10\times$  improvement in the gate volume, exceeding the  $0.99\times$  of SS<sub>o</sub> and  $1.03\times$  of GF<sub>o</sub>.

## 6.2 Zooming into individual groups

We now turn our attention to understand the impact of our qubit mapping methods within each circuit size group. Due to the large number of groups and configurations, we focus on two groups, G2 and G5. Figure 3 displays the normalized circuit depth for the 4 corresponding configurations of topologies and compilers. We can see the individual behavior of the 15 circuits comprising group G2. Our mappings used with the QISKIT compiler clearly provide better benefits than when using TKET on Manhattan’s group G2 (Figure



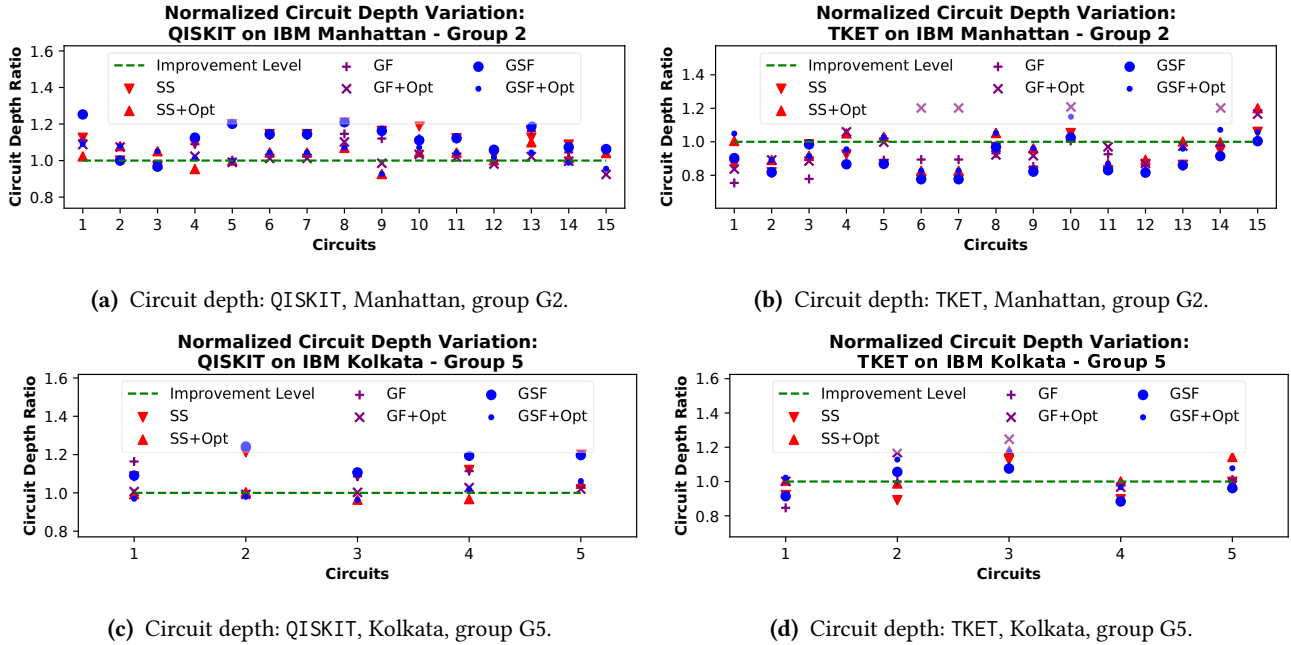


Figure 3. Normalized circuit depth variation in IBM-QX, groups 2 and 5.

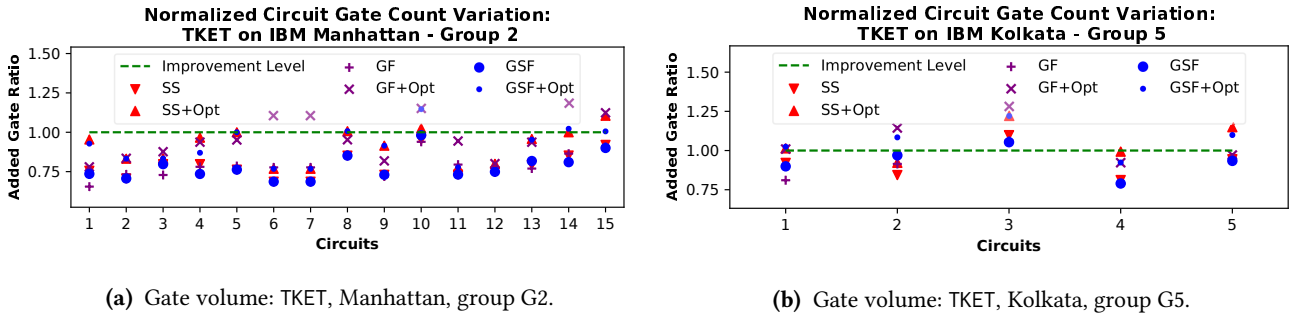


Figure 4. Normalized gate volume variation in IBM-QX, groups 2 and 5, only TKET compiler.

3a). More specifically, we can notice that  $GSF_b$  constantly achieves the best improvement, with only one exception,  $SS_b$  at  $x$ -tick 10. We also observe that  $GSF_b$  outperforms  $GSF_o$  in all but two situations ( $x$ -tick 2 and 3). Results for the same topology and group, but this time using TKET are not as good (Figure 3b); The best improvements are obtained by the  $GF_o$  mapping in 4 cases, while the vast majority of data points fall below the improvement level. We believe this is owed to TKET being more highly tuned for smaller circuits, i.e. groups G1 – G3. Very similar trends can be observed for group 5 on Kolkata, with QISKIT achieving close to  $1.2\times$  improvement on the circuit depth in several instances (Figure 3c), and producing benefits for 3 of the 5 circuits with TKET (Figure 3d). Next, we shift our focus to analyze the impact of our mapping techniques on the gate volume. These results can be seen in Fig.4. In general, we see that the *optimized*

circuits practically always obtain better gate volumes for both topologies and both selected groups (G2 and G5). Interestingly, we also note that TKET’s gate volume results are generally worse on smaller circuits than with larger ones. This observation aligns well with results on the circuit depth metric previously discussed. Lastly, the 1.63% reported improvement (Sec. 1) in gate volume was obtained in group G3, Kolkata device, with TKET.

### 6.3 Impact on SWAP operations

To conclude our evaluation, we present in Fig.5 plots showing the impact of our mapping strategies over quantum circuits consisting from 500 QOPS to 100K QOPS. This range spans parts of group G1 and all of groups G2 – G7. Data points are sorted by their original circuit size, i.e. the number of QOPS prior to compilation. Data clearly demonstrates that our qubit mapping approach significantly reduces the

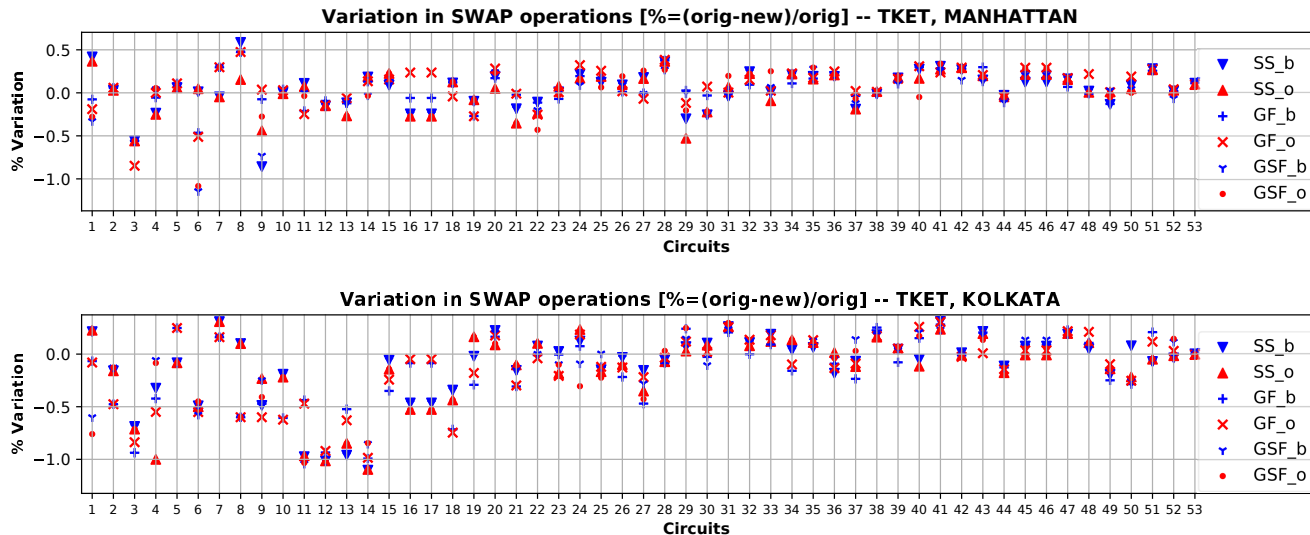


**Figure 5.** Impact of new qubit mappings on SWAP insertion with TKET: Manhattan (top) and Kolkata (bottom) devices.

number of SWAPs when used with TKET, nearing 50% SWAP reduction in a few occasions, and consistently reaching 30% to 40% reduction for large enough circuits. Especially noticeable is the trend change after the first 10 circuits, where our results experience a marked improvement on Kolkata, and especially on Manhattan, as the circuit size increases. In addition, the fact that all our mapping variants improve collectively further strengthens the premise that TKET is currently better suited for small circuits and for topologies with lower qubit counts. In contrast, improvements with QISKIT are more modest, reaching up to 15% improvement on Manhattan and 16% reduction on Kolkata (NOTE: Plot omitted due to space limitations). We also note that the *optimized* configurations (the ones with suffix *o*) consistently achieve better results than their *base* counterparts.

## 7 Related Work

The problem of qubit allocation has gained strong interest in the last few years, largely on account of its impact on several quality metrics that affect the performance and behavior of a quantum program [15]. However, this problem has been typically studied in conjunction with the *layout synthesis* task (also known as *layout routing*), which repairs a quantum program by moving qubit states onto physically adjacent qubits to meet topological constraints [13]. Furthermore, this problem has been proven to be NP-complete [20, 22]. As a result, exhaustive enumeration and search techniques such as JKU’s [25], while efficient on small circuits and small devices, will ultimately not scale with programs expected to have millions of quantum gates. Heuristics such as SABRE [12] and WPM [20], which perform multiple passes on the input program, offer better scalability prospects. In

addition to SABRE, WPM, JKU, TKET line placement [21], BMT [19], Google’s Cirq [7] greedy routing and IBM’s *Dense Layout* and *Stochastic Swap* [9], also perform qubit placement by traversing the DAG quantum graph, and performing local decisions on network layers or qubit paths. As an alternative, several works have also attempted to tackle this problem using Integer Linear Programming and Boolean Satisfiability Solvers [3, 15, 16, 22, 24]. These approaches have been successful in finding high-quality solutions to improve program success rates with noise-aware mappings. However, they still attempt to map individual gate instances, often in combination with gate scheduling. Consequently, they are more apt for small circuits and small devices. In contrast, the methods proposed in this work, in a spirit similar to [8], focus exclusively on the logical-to-physical assignment of qubits, deferring the SWAP insertion job to later passes.

## 8 Conclusion and Future Directions

We have presented two qubit mapping techniques, which can be used independently and together. We assume a decoupled strategy for qubit mapping, where pairs of offending qubits not physically connected will be repaired by a later compiler pass. More, our approach, based on detecting repetitive string patterns, often combined with global frequency detection, offers strong benefits with the QISKIT and TKET compilers, showing improvement on quality metrics such as circuit depth, gate volume and SWAP count. As future work, we plan to further exploit string-oriented quantum optimizations to find patterns that allow for the decomposition of large quantum programs, and leveraging repetitive patterns to better exploit locality.

## References

- [1] Thomas Alexander, Naoki Kanazawa, Daniel J Egger, Lauren Capeluto, Christopher J Wood, Ali Javadi-Abhari, and David C McKay. 2020. Qiskit pulse: programming quantum computers through the cloud with pulses. *Quantum Science and Technology* 5, 4 (2020), 044006.
- [2] Frank Arute, Kunal Arya, Ryan Babbush, Dave Bacon, Joseph C Bardin, Rami Barends, Rupak Biswas, Sergio Boixo, Fernando GSL Brandao, David A Buell, et al. 2019. Quantum supremacy using a programmable superconducting processor. *Nature* 574, 7779 (2019), 505–510.
- [3] Debjyoti Bhattacharjee, Abdullah Ash Saki, Mahabubul Alam, Anupam Chattopadhyay, and Swaroop Ghosh. 2019. MUQUT: Multi-Constraint Quantum Circuit Mapping on Noisy Intermediate-Scale Quantum Computers. (2019). arXiv:quant-ph/1911.08559
- [4] Vladimír Bužek and Mark Hillery. 1996. Quantum copying: Beyond the no-cloning theorem. *Physical Review A* 54, 3 (1996), 1844.
- [5] Alexander Cowtan, Silas Dilkes, Ross Duncan, Alexandre Krajenbrink, Will Simmons, and Seyon Sivarajah. 2019. On the Qubit Routing Problem. In *14th Conference on the Theory of Quantum Computation, Communication and Cryptography (TQC 2019) (Leibniz International Proceedings in Informatics (LIPIcs))*, Wim van Dam and Laura Mancinska (Eds.), Vol. 135. Schloss Dagstuhl–Leibniz-Zentrum fuer Informatik, Dagstuhl, Germany, 5:1–5:32. <https://doi.org/10.4230/LIPIcs.TQC.2019.5>
- [6] Andrew W Cross, Lev S Bishop, John A Smolin, and Jay M Gambetta. 2017. Open quantum assembly language. *arXiv preprint arXiv:1707.03429* (2017).
- [7] Cirq Developers. 2021. Cirq. (Aug. 2021). <https://doi.org/10.5281/zenodo.5182845> See full list of authors on Github: <https://github.com/quantumlib/Cirq/graphs/contributors>.
- [8] Blake Gerard and Martin Kong. 2021. Exploring Affine Abstractions for Qubit Mapping. In *2021 IEEE/ACM Second International Workshop on Quantum Computing Software (QCS) (QCS '21)*.
- [9] IBM. 2018. Qiskit. (2018). <https://qiskit.org>
- [10] IBM. 2021. IBM Quantum Services. (2021). <https://quantum-computing.ibm.com/services>
- [11] Johannes Kepler University Linz Institute for Integrated Circuits. 2019. IIC JKU - IBMQX QASM Circuits. (2019). [https://github.com/iic-jku/ibmqx\\_mapping/tree/master/examples](https://github.com/iic-jku/ibmqx_mapping/tree/master/examples) Online; accessed on April 2021.
- [12] Gushu Li, Yufei Ding, and Yuan Xie. 2019. Tackling the Qubit Mapping Problem for NISQ-Era Quantum Devices. In *Proceedings of the Twenty-Fourth International Conference on Architectural Support for Programming Languages and Operating Systems (ASPLOS '19)*. ACM, New York, NY, USA, 1001–1014. <https://doi.org/10.1145/3297858.3304023>
- [13] Dmitri Maslov, Sean M. Falconer, and Michele Mosca. 2008. Quantum Circuit Placement. *IEEE Transactions on Computer-Aided Design of Integrated Circuits and Systems* 27, 4 (2008), 752–763. <https://doi.org/10.1109/TCAD.2008.917562>
- [14] Jarrod R McClean, Ian D Kivlichan, Damian S Steiger, Yudong Cao, E Schuyler Fried, Craig Gidney, Thomas Häner, Vojtěch Havlíček, Zhang Jiang, Matthew Neeley, et al. 2017. OpenFermion: The Electronic Structure Package for Quantum Computers. *arXiv preprint arXiv:1710.07629* (2017).
- [15] Prakash Murali, Jonathan M. Baker, Ali Javadi-Abhari, Frederic T. Chong, and Margaret Martonosi. 2019. Noise-Adaptive Compiler Mappings for Noisy Intermediate-Scale Quantum Computers. In *Proceedings of the Twenty-Fourth International Conference on Architectural Support for Programming Languages and Operating Systems (ASPLOS '19)*. ACM, New York, NY, USA, 1015–1029. <https://doi.org/10.1145/3297858.3304075>
- [16] Prakash Murali, David C McKay, Margaret Martonosi, and Ali Javadi-Abhari. 2020. Software mitigation of crosstalk on noisy intermediate-scale quantum computers. In *Proceedings of the Twenty-Fifth International Conference on Architectural Support for Programming Languages and Operating Systems (ASPLOS'20)*. 1001–1016.
- [17] Rigetti. [n. d.]. Pyquil. ([n. d.]). <https://github.com/rigetti/pyquil>
- [18] Rigetti. 2021. Rigetti Systems: Aspen-9 Quantum Processor. (2021). <https://qcs.rigetti.com/qpus/>
- [19] Marcos Yukio Siraichi, Vinicius Fernandes dos Santos, Caroline Collange, and Fernando Magno Quintão Pereira. 2019. Qubit Allocation As a Combination of Subgraph Isomorphism and Token Swapping. *Proc. ACM Program. Lang.* 3, OOPSLA, Article 120 (Oct. 2019), 29 pages. <https://doi.org/10.1145/3360546>
- [20] Marcos Yukio Siraichi, Vinicius Fernandes dos Santos, Sylvain Collange, and Fernando Magno Quintao Pereira. 2018. Qubit Allocation. In *Proceedings of the 2018 International Symposium on Code Generation and Optimization (CGO 2018)*. ACM, New York, NY, USA, 113–125. <https://doi.org/10.1145/3168822>
- [21] Seyon Sivarajah, Silas Dilkes, Alexander Cowtan, Will Simmons, Alec Edgington, and Ross Duncan. 2020. tket: a retargetable compiler for NISQ devices. *Quantum Science and Technology* 6, 1 (Nov 2020), 014003. <https://doi.org/10.1088/2058-9565/ab8e92>
- [22] Bochen Tan and Jason Cong. 2020. Optimal Layout Synthesis for Quantum Computing. In *Proceedings of the 39th International Conference on Computer-Aided Design (ICCAD '20)*. Association for Computing Machinery, New York, NY, USA, Article 137, 9 pages. <https://doi.org/10.1145/3400302.3415620>
- [23] Bochen Tan and Jason Cong. 2020. Optimality Study of Existing Quantum Computing Layout Synthesis Tools. *IEEE Trans. Comput.* (2020), 1–12. <https://doi.org/10.1109/TC.2020.3009140>
- [24] Robert Wille, Lukas Burgholzer, and Alwin Zulehner. 2019. Mapping quantum circuits to IBM QX architectures using the minimal number of SWAP and H operations. In *2019 56th ACM/IEEE Design Automation Conference (DAC)*. IEEE, 1–6.
- [25] Alwin Zulehner, Alexandru Paler, and Robert Wille. 2018. Efficient mapping of quantum circuits to the IBM QX architectures. In *2018 Design, Automation Test in Europe Conference Exhibition (DATE)*. 1135–1138. <https://doi.org/10.23919/DATE.2018.8342181>